arXiv:1207.7018v1 [physics.ins-det] 30 Jul 2012

# Scalable design of an IMS cross-flow micro-generator/ion detector

**Juan J. Ortiz**[1] , **Guillermo P. Ortiz**[2], **Christian Nigri**[1], **and Carlos Lasorsa**[1]

[1]Comisión Nacional de Energía Atómica, Av. Gral Paz 1499, CP 1650, San Martín, Pcia. de Buenos Aires, Argentina
[2]Dto. Física, Fac. Cs. Exactas, Nat. y A. - Inst. Mod. e Innov. Tec. - Universidad Nacional del Nordeste, Av. Libertad 5450 Edificio B, W3404AAS, Campus UNNE, Corrientes, Argentina

E-mail: `jjortiz@cnea.gov.ar, gortiz@exa.unne.edu.ar`

**Abstract.** Ion-mobility spectrometry (IMS) is an analytical technique used to separate and identify ionized molecules in the gas phase based on their mobility in a carrier buffer gas. We present a design for generation and detection of ions that might resolve an issue related to limitations at sub-millimeter scales of cross flow method applications. Introducing a lobular ion generation localized to a few ten of microns, and a substantive simplifications of design, we make an integrated device for ion micro-generation and its detection. Main advantage of this design is their scalability that allows further control for compounds identification.

*OMS design, gases detectors, cross-flow, micro-devices*

PACS numbers: 41.75.-i, 42.82.Cr, 52.80.Hc, 85.40.-e

## 1. Introduction

Ion-mobility spectrometry (IMS) is an analytical technique used to separate and identify ionized molecules in the gas phase based on their mobility in a carrier buffer gas. IMS devices come in a wide range of sizes (often tailored for a specific application) and are capable of operating under a broad range of conditions, but not at submillimeter or milimetric scale. In-situ detection with those devices are heavily employed for military or security purposes, such as detecting drugs and explosives. This technique is based on ion mobility property that ions acquires from mass, charge, size and shape when they moves through a gas due to its interaction with an electric field, with drift velocity

$$v_d = KE, \tag{1}$$

which is proportional to the electric field of strength $E$. The ion mobility

$$K = \frac{3}{16}\frac{ze}{N}\frac{1}{\Omega_0}\sqrt{\frac{2\pi}{k_b T}(\frac{1}{m}+\frac{1}{M})}, \tag{2}$$

defines the compound to be identified, since its dependence to thermal fluctuation $k_b T$, electrical charge $ze$, gas density $N$ and collision cross-section $\Omega_0$ can be obtained from the balance between mobility and diffusion force during elastic collision between the $m$ mass ionized molecule and a neutral $M$ mass molecule [1]. Roughly speaking, in conventional IMS devices, drift-time

$$t_d = \frac{d}{v_d} = \frac{d}{KE} \tag{3}$$

defines the type of molecule to identify. Mobility $K$ of each sample is obtained by establishing the field $E$ and distance $d$, predetermined by the experimental device's configuration.

## 2. Standard cross-flow

Usually, determining time-of-flight to identify an analyte via traditional IMS requires $d$ in Eq.(3) to be hundreds of mm [2]. Spectroscopy in two orders of magnitude below represent an unresolvable issue via this technique. Alternatively, cross-flow method [3] employs an ion-impulsing field, but transversal to corresponding to the traditional IMS, which allows to split a stream of ions according to their mobility. This design is remarkably compact and relatively easy to manufacture with micro-system technology. As ionized particles are detoured with a field in transversal direction to the flux of a carrier gas, two mobility vectors are obtained: one in the flux's direction and the other one perpendicular to it, generated by an electrostatic field [1, 4]. Cross-flow method with differential detection [5] allows mobility identification via determination of bounds with maximum mobility measures. Fig. 1 shows an scheme of that device with a radioactive source which produces ions in such a wide area that it covers the whole entrance to the detection zone. A carrier flux moves charged particles from the ionization zone to the latter, where an electric field deflects the ions and those with higher mobility will be collected within the first electrode (detector). Maximum detectable mobility $k^b_{\max}$ for next electrode is defined by corresponding mobility for ions that entering into the channel at its lower part $(x = x_0, y \approx 0)$, reach position on detectors $(x = x_b, y = h)$, being $h$ channel height. In *ideals* ion condition, the coulombian repulsion between ions and the diffusive effects are minimum, then it

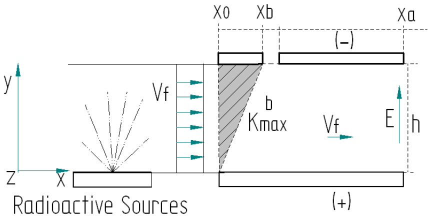

**Figure 1.** Diagram of differential detection for flat detectors with radioactive ionization source. The velocity of the fluid is assumed constant $v_f$ in the channel. Between the bottom electrode (anode) and the upper electrodes separated a distance $h$ applies a potential difference which generates an electric field $E$, we assume uniform. $x_b$ and $x_a$ end positions determined by the sizes of the detectors and the magnitudes of the vectors of field and flow are designed to detect maximum levels of mobility (see text).

will only be possible to collect ions with lower mobility than $k^b_{\text{max}}$ in the following detectors, since the ones with higher mobility will be collected within the first detector, regardless of their position entering into the channel.

This detection method has an inconvenient; ions meant to be detected might be caught by more than one detector. In other words, one can only be sure that, in a latter detector, mobility is bounded by a maximum value. This problem, and how to solve it, is clearly explained in an example involving two unique mobilities in Fig. 2, showing the path of two ionized molecules, a sample and the carrier. The

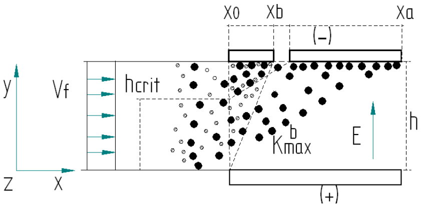

**Figure 2.** Diagram of a gas detection (black circles) and gas drag (smaller scratched circles), the ions are distributed in the channel, the charged particles that are above the height $h_{crit}$ will produce overlap in the detection signal.

one with higher mobility is represented with scratched circles, which corresponds to some ionized molecules of the carrier gas. Black circles represent the ions of the sample gas to be detected. Assuming the length of the first detector, carrier flux, and potential difference between anode and detectors are set for $k^b_{\text{max}}$ to be equal or close to the carrier gas mobility, it can be reassured that all the carrier gas ions are collected within the first detector. However, lower mobility ions may be caught in any of both detectors. Clearly, and disregarding coulombian repulsion between ions and diffusive effects, there is a critical height $h_{\text{crit}}$, for which all the molecules' ions with lower mobility that are traveling above $h_{\text{crit}}$ will be caught by the first detector. Thereby it's not possible to set a particular detector for the particles to be identified. To counter this effect, the bibliography proposes establishing a size relationship between electrodes, which determines an error only acceptable with a substantial rise in the device's size [5], that would be contrary to our search for scaling. Although, yes there should be desirable solutions that allow to separate mobilities via micro-system design. Cross-flow system employs an unique carrier gas to move the ions whereas the traditional IMS method employs gate aperture and closure to define initial measurement time[6]. This method requires a higher amount of unscalable elements, for example, an arrangement of potential rings to move charged particles from the ionizers towards the detectors [7]. Besides, traditional IMS employs an injected counter-current gas [8] which would be very hard to apply on a submillimeter scale due to the rising viscosity effect, as explained in Section 3. Nowadays, there are ways to solve said issue, such as focalization [9]. In the above discussion, concept for focalization means to do something equivalent to avoid ions traveling with height larger than $h_{\text{crit}}$. Then, in our example, the sample ions would be collected only at the second detector, which is a kind of condition needed for identification proposes. It's been utterly expensive and complex to apply this kind of solutions so far, because of the inconveniences submillimeter scale brings. In standard cross-flow devices, funnels or intrincated channels can be implemented to narrow down the flow inside the system, thus generating turbulence and stopped flow zones. Results reports loss of identification efficiency for these kind of devices [10].

Our main research hypothesis centers on focalization being possible implicitly via a ionizer's geometric design that allow to generates ions all in a size smaller enough than $h_{\text{crit}}$. Applied to the example above, all this localized ions will travel at height smaller than $h_{\text{crit}}$, then no nozzle are needed in order to do sample ions would be collected only at the second detector. In Sections 4 and 5 we will present an experimental design setup and their analysis for doing a localized or lobular ions generation. But, now in the following Section 3 we shall describe how to deal with the transport of ions which again also will concern to ion micro-generation design.

## 3. Localized ions and cross-flow

We propose a solution for control positions of collected ions described in Section 2 via ion micro-generation in a cross-flow system type by using a fluid to move localized generated charged particles. In that Section the advantages of cross-flow model due to its lower component amount are mentioned too. Considering Ecs.(1), (2) and (3) can only be applied in a non-turbulent regime, we will now analyze how the fluid travels along the channel. For that matter, a constant rectangular section is proposed, without any detours nor expansions or contractions within the fluidic vein. Taking this into account, we verify first the laminar flow by using the Reynolds number, which we estimate for non-circular sections, as

$$R_D = \frac{4R_H\, v_f}{\nu} \tag{4}$$

in term of the $\nu$ cinematic viscosity and hydraulic radius $R_H = wh/2(w+h)$, the ratio between the fluid normal section area and its perimeter, where $w$ is the channel width. The flow rate $Q$ is implicit in the above equation, because it is estimated as the average velocity of flow $v_f$ multiplied by the section of the channel, i.e. $Q = whv_f$.

For the sake of design, a significant size reduction was made for $h$ and $w$, ergo, we are looking for $Q$ to be low enough so $R_D < 2000$, that is enough for laminar condition of fluid regime. However, $Q$ can not be too low – if it were, the number of

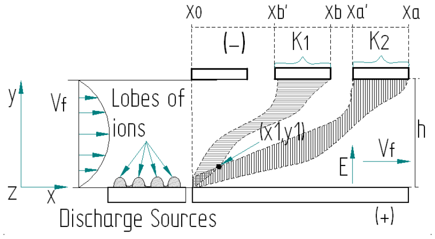

**Figure 3.** Longitudinal cutting of the channel with localized production of ions (lobes of ions) and the trajectory that follow these particles within the detection area. Due to ion localization, generated flows results on stream of ions with small sections like focalized ions. Under laminar flow conditions field $E$ drifts ions doing the stream reaching the detectors. For ions with larger mobility $K_1$ between positions $(x_b, h)$ and $(x'_b, h)$ closer to the entry that ions with smaller mobility $K_2$ at farther positions between $(x_a, h)$ and $(x'_a, h)$.

ions would be too small during analysis. Also, channel longitudinal dimensions have to be smaller enough so the lifespan of generated ions is longer than time they take to arrive to the detection zone. All this together allows establishing a higher velocity and dimension range that can be optimized in a way that helps obtaining an efficient functioning with its possible smallest size[12].

Detectors position and dimension in a localized ion generation system are calculated by estimating charged particles' trajectory. Our hypothesis on a localized ion generation and flow laminarity means generated ions access detection zone with height $y \approx 0$. For a constant carrier flow, there are two orthogonal components for ion movements in the detection zone: constant flow velocity $v_f$ and drift velocity $v_d$ Eq.(1). Therefore, considering an ion from $(x_0, 0)$ takes the same time to arrive to the detector in $(x, h)$ for each movement direction, we obtain:

$$x - x_0 = \frac{v_f\, h^2}{K\, V} \tag{5}$$

where the drift field can be estimated by $V/h$, assuming border effects are negligible and electric potential $V$, applied on the detectors, generates a uniform field in the detection zone. Considerations on a more realistic situation will be taken in the next Subsection 3.1, however, and regardless of trajectory details for a laminar flow, how focalization works to separate two species with different mobilities can be explained with the following example: For ions with mobility $K_1$ and $K_2$ both with same initial location defined by a stream of ions with lower position $(x_0, 0)$ and higher position $(x_0, h_0)$ they travels as shown by two sketched stream in Fig. 3 and arrive at positions $(x_b, h)$ and $(x'_b, h)$ for ions with mobility $K_1$ and $(x_a, h)$ and $(x'_a, h)$ for ions with mobility $K_2$, Fig. 3 shows streams from generated lobes of ions to detector collections which starts in $(x'_b, h)$ with length $x_b - x'_b$ for ions with $K_1$ mobility higher than $K_2$ mobility ions that are detected from $(x'_a, h)$ and has $x_a - x'_a$ length. Clearly, ion stream will not overlap on detectors and required separability will be verified as long as trajectory of ions of the lowest side of stream of ions with larger mobility and trajectory of ions of the higher side of stream of ions with smaller mobility meet at a lower height than channel $(h)$. Having defined a such meeting point $(x_1, y_1)$ for these trajectories in plane $xy$ displayed on Fig. 3 and assuming uniform velocities as in

Eq.(5), we can estimate

$$x_1 - x_0 = \frac{v_f\, h}{K_1\, V} y_1 = \frac{v_f\, h}{K_2\, V}(y_1 - h_0). \tag{6}$$

Being potential $V$ and flow velocity $v_f$ same for both molecules we propose that separability will be guaranteed provided that $y_1 \leq h$. Therefore, in case $y_1 = h$ we find a bound for the maximum localizing size

$$h_0 = h(1 - \frac{K_2}{K_1}), \tag{7}$$

needed to separate two ionized molecules according to their mobilities and channel height. Our research's main hypothesis centers on focalization being possible via the ionizer's geometric design. Eq.(7) provides a bound for the scaling of that focalization with the detection device's size that allows the identification of the species. This scalability requirement has driven us towards micro-system technology and the originality in our proposal lies on the solution reached.

### *3.1. Parabolic approximation of velocity*

The flow is generated by the pressure difference between the device's entrance and exit, $P_1$ and $P_2$, respectively. Velocity is modified by friction between the fluid and the walls, and glide of idealized layers of fluids. Assuming irrotational and incompressible fluid's conditions and fits the device wall's static conditions to analyze dependence on vertical direction, we obtain by force equilibrium

$$v_f(y) = \frac{P_1 - P_2}{4\nu L} y(h - y), \tag{8}$$

where $L$ is the channel length and $y$ is the height variation for the channel that goes from 0 to $h$ as defined in Section 2.

In order to investigate the velocities profile's role in a submillimeter scale we take into account numeric simulation for the trajectory in a plane $(x, y)$ of *ideals* ions with the same mobility as Nitrogen when impulsed in $x$ direction acquiring a $v_f(y)$ of Eq.(8) due to $P_1 - P_2 = 5.35\ 10^{-5}$ dyne / $\mu$m$^2$, $L = 7.5\ 10^4\mu$m and $\nu = 1.822\ 10^{-12}$dyne s/$\mu$m$^2$ and impulsed in $y$ direction acquiring $v_d$ given by Eq.(1) for $K = 2.2\ 10^8\mu$m$^2$/Vs due to a potential difference of 9 and 18$V$ between flat detector electrodes (anode and cathode) separated $h = 10^3\mu$m. In Fig.4 trajectories are shown for two initial positions (0,0) and (0,50$\mu$m) that would represent limit cases due to localizing of ions, illustrated in Fig.3 and now calculated for parabolic profile resulting a narrow laminar stream. For the uniform profile, trajectory for initial position (0,0) is shown too. It is not shown in Fig. 4 the trajectory for (0,50$\mu$m) because being for the uniform profile it belongs to a parallel line separated 50$\mu$m from the first one, defining a straight laminar stream. Standard cross-flow method belongs to the scale of ten of mm [5] where the change of the velocity profile due to viscosity effect is negligible. However, for submillimeter scale for detection position and detector's size designs, an error as high as the channel's height can be made when not taking into account how velocity depends on it's height. Note that when duplicating applied potential ions are detected at half the corresponding length for the lower potential case. This is due to inverse proportionality Eq.(5) between horizontal position detection and potential applied to the detector, that approximately is verified here when a such viscosity is taken into account.

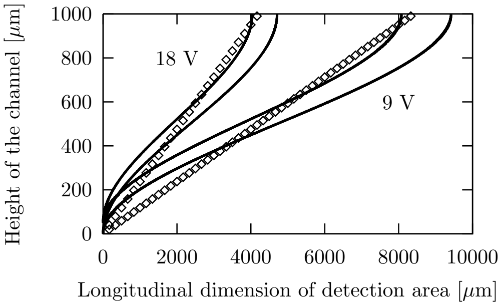

**Figure 4.** Numerical simulation of trajectories for ions in the area of detection when you apply $9 - 18V$ potential differences between cathode and anode. Continuous line for the parabolic profile Eqs. (8) and (1) for two initial positions (0,0) and (0,50$\mu$m). Also shown in dashed dotted line a uniform profile with initial position (0,0).

## 4. Description of the proposed micro-device

Our device has been designed while considering position and direction of the mobility vectors for the ions, from generation and transportation until detection. This was made possible via electric discharges, the transport fluid's flux and detection electric field. But, we have taken orthogonal directions for each other in order to minimize effects of influence between them. By employing a virtual model of the micro-device via CoventorWare software [11] we made the design shown in Fig. 5. With lift off, the design proceeds, on a glass substrate a positive photo-resin is deposited and protected with a plastic cover, containing the target structure's image. With UV light, resin is modified in unprotected places, so unmodified resin can be removed with the cover as well. Via an anodic deposition process [13] a copper layer is applied over all the substrate. Finally, the resin layer on the first step is removed by using Acetone and the geometry of the metal layer remains on the substrate. This manufacturing process has been used because of its flexibility and sturdiness. The software allows the simulation of the model construction from optic layers and manufacturing process [14].

The point of this work was obtaining a minimum size compact sensor, with low cost and simple manufacture. This micro-device has two main zones. One is the ionization zone, where lobes of ions are generated by employing a special kind of electric discharge which will be explained in the following Section 5. Via a carrier gas, those charged particles of the sample are transported to the detection zone. There are detectors immersed in an electrostatic field that deflects and separates ions according to their mobility. In Fig. 5 these two zones are shown in detail. In the front of the ionization zone, two guides that drive the sample and the carrier gas are shown. The guides determine separation distance between two substrates; in Fig.5 only the inferior substrate is shown. After entering, carrier gas and sample run through the device towards the ionization zone, consisting on six sources mounted on the inferior substrate's surface. Each source has seven pairs of flat metallic electrodes, in front of each other with a separation of 40$\mu$m. The anode has six triangular tips, separated 300$\mu$m between each other and a flat cathode. Distance between sources is 1500$\mu$m and the last one is 540$\mu$m away from the detection zone. These can be individually connected across the connection electrodes, shown in Fig. 5 as (2) and (8) respectively.

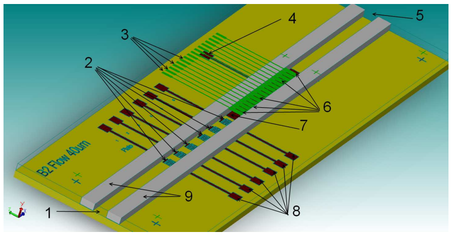

**Figure 5.** Model in three dimensions of the proposed micro-device. The carrier gas mixing and sample enters a guide determined by two guides (9) and two substrates (1) (only displayed bottom substrate). In the area of ionization, six sources mounted on the surface of the bottom substrate, can connect individually (2) through (8) connection electrodes. The detection zone has mounted over the bottom substrate a single connection (4) flat electrode (7). Sectioned flat electrodes (6) that connects individually (3) are mounted on the top substrate. The carrier gas comes out of (5).

Detection zone has a flat electrode with a lone connection mounted on the inferior substrate. On the superior substrate, sectioned flat electrodes are mounted, which are connected individually; each being 900$\mu$m long and being separated 100$\mu$m, as shown by (6) and (3) respectively in Fig.5. Total channel length is 7.5 $10^4\mu$m but the maximum active zone is below 50% of said value. Channel width is 2 $10^3\mu$m and height is $10^3\mu$m. With these dimensions and an air stream of around 0.33 $10^{14}\mu$m$^3/s$ we estimate a flow in laminar regime due to $R_D \approx$1000.

## 5. Ion micro-generation

The ion generation issue is faced via localized production of a self-limited discharge, or corona discharge, that will help produce the amount of sample's ions needed to be identified. Electric discharges due to dielectric rupture can be reached via enough energy accumulation between electrodes laid to an electrostatic potential difference [16]. For our own use, the previous state in which luminescence beings, also known as corona discharge, is just enough to ionize the sample. Therefore it is possible to develop the electric field and the electric potential before the electric discharge by solving the Laplace equation in a volume defined by a closed surface. Let us consider the proposed configuration [17] of two concentric cylindrical conductors as shown in Fig.6 to analyze the corona discharge. The outside is hollow, with a minimum $S$ radius and the inner has $r$ radius. The inner cylinder is kept in a $V$ potential and the outer cylinder in a zero potential. Clearly, this configuration is different from the tip and plate one and the two parallel conductors separated a $2S$ distance. However, it is possible to verify solutions for the Laplace equation are similar in all of those cases [18], being electric potential

$$\phi(x) = V\frac{\ln(S/x)}{\ln(S/r)}, \tag{9}$$

where $x$ represents radial distance from the center of the inner cylinder to an arbitrary point in the space between both cylindrical conductors. Then,

$$E(x) = V\frac{1/x}{\ln(S/r)}, \tag{10}$$

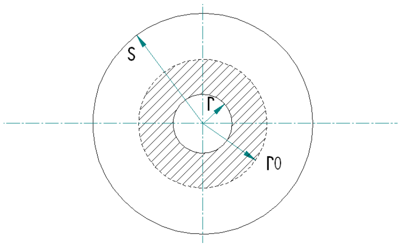

**Figure 6.** Settings to evaluate the discharge corona. Two concentric conductor cylinders of radius $r$ inner and radius $S$ external, between the two cylinders is the dielectric that we want to ionize. The grated area of radius $r_0$ marks the boundary of ionization zone.

is the module for the radial electric field, orientated from the inner conductor (anode) outwards (cathode). In size systems of ten of mm or bigger, empirical Peek's law [19] establishes the necessary electric potential in the anode to witness a corona discharge: At a distance proportional to the square root of the anode's radius, the produced electric field must equal the necessary field $G_0$ for the rupture of the dielectric it is embedded on. For the case of air $G_0$=3 V/$\mu$, which from Eq.(10) and according to Peek's law

$$E(r + 0.301\sqrt{r}) = G_0, \tag{11}$$

allows to determine critical potential on the anode

$$V_c = G_0\, r \ln(S/r) \left(1 + \frac{0.301\sqrt{cm}}{\sqrt{r}}\right) \tag{12}$$

necessary to begin the corona discharge. The $\sqrt{cm}$ factor which goes along with 0.301 is due to the units of choice to measure distance. Right panel of Fig.7 shows the electric field foretold by the model on anode surface $G_c$ depending on $S/r$ for an applied potential on that electrode $V_c$ =415 V corresponding to the value made explicit by Peek's law for $S/r = 3.2$ and $S = 40\mu$m. Since the magnitude of the field decays with distance from the anode, $G_c$ must be higher than $G_0$. Fig. 7's right panel shows that for this case, field $G_c \approx 10G_0$. The question is what size should be dimensions for

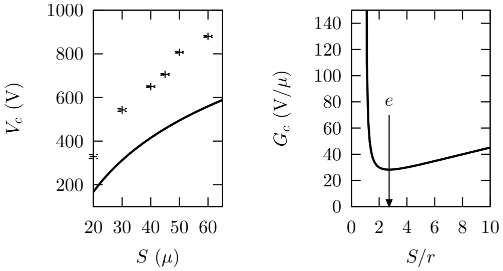

**Figure 7.** Left panel: critical potential as a function of $S$ for a radius of curvature of the tip $r = 12.5\mu$m. At continuous line analytical model Eq. (12). Cross points corresponds to the experimental determination using Nitrogen gas. Right panel: intensity of the electric field on the anode as a function of $s/R$ when the voltage applied on it is $V_c = 415$ V.

such geometric that ensures discharge to be self-limited. The analytic results, Fig.7, show that it is only possible if $S/r > e$. Otherwise, as $G_c$ has a minimum in $S/r = e$, a rise in anode effective radius $r_0$ as indicated in Fig.6, associated with a very early stage of the discharge, would mean $S/r < e$ and a huge rise on the surface field which would favor the started phenomenon and the discharge would remain until the total rupture of the dielectric, becoming an arc-type of discharge regime. When $S/r > e$, any effective increase in $r \rightarrow r_0$ means a diminished surface field and eventually, a smaller field than established by Peek's law, producing a self-limitation on said phenomenon.

The left panel on Fig. 7 shows critical potential for Nitrogen gas varying separation distance $S$ for a fixed curve radius $r = 12.5\mu$m. The analytical model from Eq.(12) foretells a tendency of critical potential to rise along with $S$ but shows a systematic difference by underestimating critical potential. This is reasonable because the analytical model requires $S \gg r$ for the tip's geometry and surroundings not to be a main factor in the electrostatic solving of the issue. To relax this approximation and to investigate if Peek's law is valid in the micro-scale, we numerically calculate the electric field inside the ionization volume defined in Section 4 and solving the Laplace equations [27] for the configuration displayed in Fig. 8 e). The left panel shows the electric field's magnitude on a section of the channel that goes through the tip of the central triangular anode. Applied voltage corresponds to critical values experimentally determined for Nitrogen gas, $V_c = 650, 706, 807$ and 880V and $S = 40, 45, 50$ and $60\mu$m, respectively. Curvature radius $r = 12.5\mu$m is the same for every case. We found it is possible to establish a common distance $r_0$ from the origin of the curvature radius that determines the tip of the anode up to the surface that defines a volume where $E \geq 3$ V$/\mu$m. If Peek's law is verified for this scale, this distance should be similar to effective radius $r_0 \approx r + 30.1\sqrt{r}$, measuring the curvature radius in micrometers. This prediction becomes true with a 10% sampling error in every case.

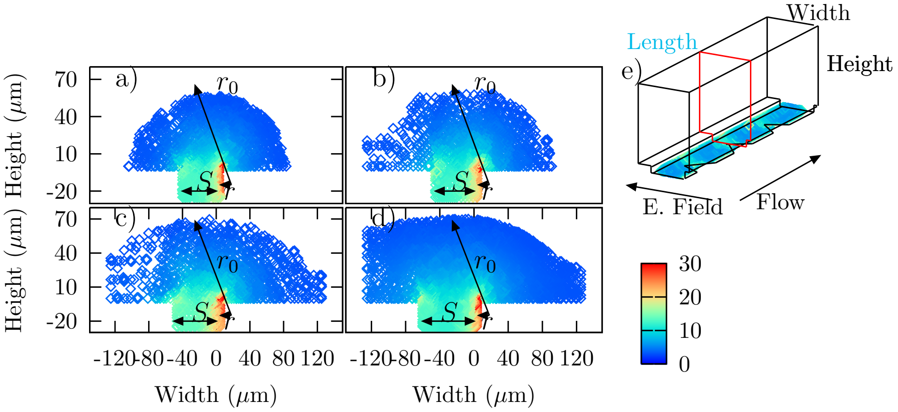

**Figure 8.** Magnitude of the electric field in V $/\mu$m for a) $S = 40\mu$m, $V_c = 650$ V; b) $S = 45\mu$m, $V_c = 706$ V; c)$S = 50\mu$m, $V_c = 807$ V; d)$S = 60\mu$m, $V_c = 880$ V on the section indicated by the outline in red within the volume of the channel (e). At the bottom of that volume is plotted the magnitude of the field in longitudinal direction at a height of $20\mu$m from the plane on the upper part of the anode and cathode. The radius of curvature $r = 12.5\mu$m of the three prongs that form the anode is the same for all cases in which varies $S$. Effective radius $r_0$ is average distance in which the electric field falls to $3V/\mu$m from the anode.

Left panel of Fig.9 shows a picture of a portion of the ionizer made of copper on a glass substrate. In the lower part there are three tips with a curvature radius of $r = 12.5\mu$m separated $S = 40\mu$m from the cathode and $300\mu$m between each other. Such a distance between two consecutive tips is enough to avoid a remarkable effect of the electric fields between tips. We have used Warburg's law [22] by an estimation of this distance according to geometric parameters for the tip and plate configuration. The right panel is a photography that show luminescence produced by these three tips when applying a potential difference between cathode and anode $V_c = 650V$. Observing said luminescence allowed experimentally establishing critical potential for the earlier mentioned cases to validate Peek's law [23] on the micro-scale.

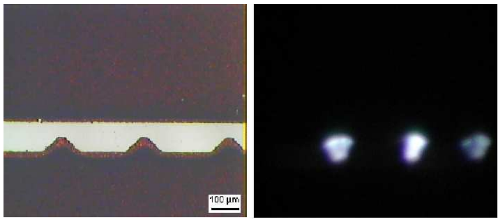

**Figure 9.** The image on the left shows a portion of the Ionizer for the experimental model built in copper on a substrate of glass designed according to the geometry shown in Fig. 8. The image on the right is a photography of the electric discharge that occurs between the electrodes when $S = 40\mu$m, $r = 12.5\mu$m, $V_c = 650V$

## 6. Results

Nitrogen is flowed first through the device's channel. Its flow is controlled through a regulator. Then, a pulse generator is connected to a $650V$ DC source – each pulse has a duration of $50\mu$s and interval between pulses is $5ms$. We analyzed the ions charges $C$ by connecting a LV 8 Keithley 6514 electrometer serially to the detection arrangement cathodes. It is connected to the electrometer as shown in the upper panel of Fig.10 and the accumulated charge is measured in a $20s$ interval. The average is calculated on ten measures for each electrode. Data dispersion according to the average is lower than 3 %.

Fig. 11 shows charge $C$ normalized with $C_0$ depending on the flow in the device and cases in which detection potential is fixed at 9 and $18V$. Reference value $C_0$ corresponds to the same experiment but with an opposing air stream. This reference is needed because the electrometer's sensibility is high enough to capture spurious signals during the experiment, for example, signals produced by generation of ions. Established parameters in these experiments correspond to the theoretical example analyzed in Subsection 3.1. Thus, the highest amount possible of charge must be obtained for $2l/min$ flow rate, and lower it to less than half, then, when risen to $5l/min$. It is to be noticed that the difference of the 45% with higher signal for $18V$ is consistent with our theoretical model as well, since when concentrating detection towards half the detection zone's length there are higher chances of collection ions. For the sake of a higher signal for 18V there is also the lifespan of ion, since they are collected approximately in half the time than 9V. For the cases in which the flow is $5l/min$ and $10l/min$ there is a transition towards the turbulent regime. Therefore,

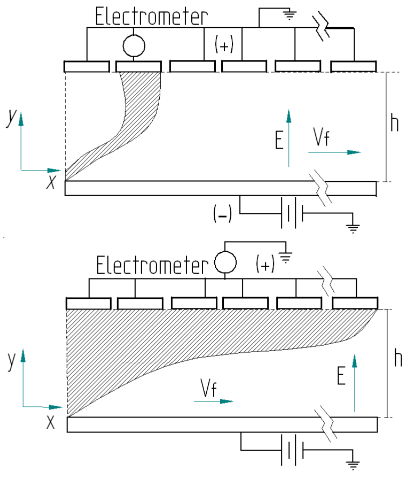

**Figure 10.** Charge measurement configuration using an electrometer. Upper panel is a measurement of the total charge as function of flow rate. Lower panel is for the charge on each detector is measured.

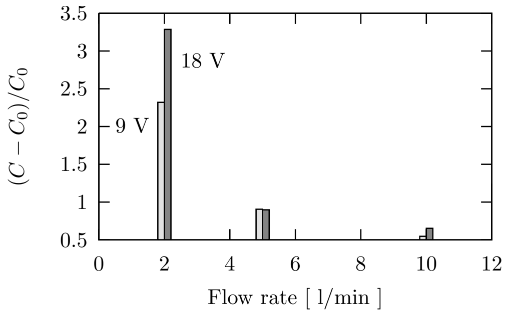

**Figure 11.** Charge signal $C$ normalized to charge $C_0$ depending on the flow rate for $2, 5, 10$ $l/min$. Clear (dark) gray bars correspond to $9V$ ($18V$).

remarkable signal differences for these flows are not expected for 9 or 18V because of the laminarity loss established for predictions in Section 3

We verify if localized lobular generation is enough to allow ionic separation via the electrometer connected as shows the lower panel in Fig.10. Fig.12 shows the charge signal $C$ measured in each detector separately, and normalized with $C_0$, for a $2l/min$ flow rate. Signal $C_0$ is obtained for each determination, same as before, by a streaming in opposing flow. The result is shown for four different detection tensions $9, 18, 28$ and $46V$. If compared to the result in Fig.4 on the numeric simulation for 9 and $18V$ and keeping into account detectors' dimensions of the micro-device on Section 4, we may observe signal maximum values obtained at positions where the detectors on the foretold distances are. According to Eq.(5), there is an inverse relationship between detection positions and applied potentials. For this reason we can observe that, by duplicating applied potential (9V) into 18V, the position of the detector that concentrates the respective signal is halved, ergo the model's prediction

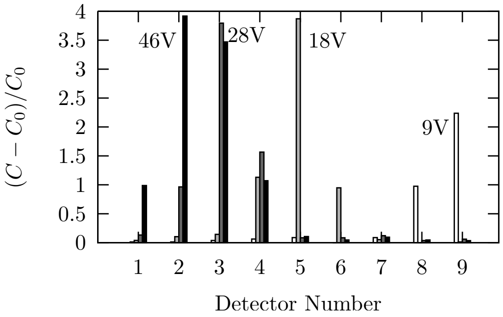

**Figure 12.** Charge signal $C$ normalized to the charge $C_0$ for flow of 2 $l/min$ as function of the number of detector. Bars in white for $9V$, light gray for $18V$, dark gray for 46, and black for $28V$.

is experimentally verified. For this same reason, when it's tripled ($\approx 28V$) the signal in the detector is obtained at the one third of the corresponding distance, and when quintupled ($\approx 46V$) the signal is almost at one fifth of those distance. This prediction is strictly accurate for an ideal case of uniform profile. For the most realistic case there is a small correction with collection distance predictions higher than established by Eq.(5) in agreement with our discussion at the end of Subsection 3.1. We note that the experimental verification of the model is due to a correct focalization by local ion micro-generation during these experiments. According to our analysis in Section 5 with the proposed experimental configuration, it is possible to determine an ionization volume with its diameter up to 10% of the channel's $h$ height. But clearly, if more localizing is required, work should be done as in Section 5 but shrinking the curvature radius of the ionizers. Regarding separation by mobility, we could state performed experiments for different potentials and one compound, at least ideally, the issue within four compounds and one potential could be mapped. This is because, channel height being constant, we approximated $E$ with $V/h$ in Eq.(1) and drift velocity depending only on the product of mobilities and applied electric potentials. Therefore, if we wanted to map results from Fig.12 to the separation by mobility, it would mean considering changes in which these would duplicate, triplicate or quintuplicate. However, expected changes between mobilities are considerably smaller. For example, between Toluene and Nitrogen, mobility changes about 24%. Usually, mobilities of the compounds to be separated are in such a range than differences are even smaller. Fig.13 shows numeric simulation of the trajectory when a $18V$ tension is applied to the detectors and a carrier flux rate of $2l/min$ is put. In the upper part of Fig.13 it can be seen that our design allows to separate, without considerable overlapping , signals corresponding to Nitrogen and Toluene. According to our analysis in Section 3.1 and employing Eq.(5), we can estimate that, for $18V$, a mobility rise of 24% would be equivalent to an average displacement of an ion current from the middle part of the fifth detector to the left by $870\mu$m. Being this distance slightly bigger than the diameter of whichever ion streams reaches that position, both ion streams before and after displacement should be across them, thus obtaining two clear signals on the detectors. This result is consistent with our prediction in Section 3 on scaling between ion current diameter at the entrance of the detection zone and at channel height. With our design, $h_0/h \approx 0.1$ and Eq.(7) is verified for Toluene and Nitrogen. On the

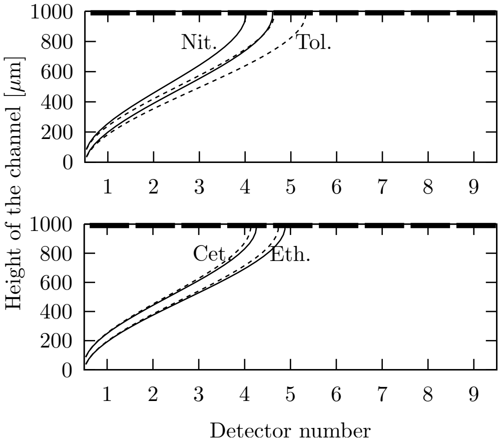

**Figure 13.** Ideal trajectory of the ions when it is applied a voltage of $18V$ and drag flow rate of 2 $l/min$ to reach the detectors. The dimensions and other parameters are the same as the experimental device. In the upper pane (bottom) displays for Nitrogen and Toluene (Acetone and Ethanol).

contrary, employing the same configuration and with differences between percentage's mobilities, as in Acetone and Ethanol cases, the scaling condition in Eq.(7) won't be verified and separation signals would overlap considerably between ion currents, as shown at the bottom of Fig.13.

The main advantage of our proposal is its scalability, which depends on the required application. For example, applying Eq.(7) for Ethanol and Acetone whose differences between mobilities are 3.4%, a bound for maximum dimension of 30$\mu$m for the initial diameter of the ion stream is obtained. Scaling the sizes of the initially proposed device an order below in a way that localization is less than maximum bound foretold, it is possible to obtain separation as verified in the simulation which result as shown in Fig.14. It also shown in Fig.14 ideal trajectories of ion streams to Acetone

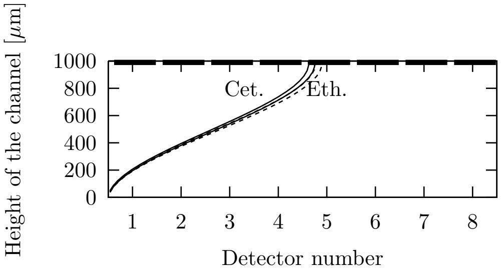

**Figure 14.** Ideal trajectory of ions of Acetone and Ethanol when it is applied a voltage of 180V. The length of each detector is 100$\mu$m. The localization of ion micro-generation is concentrated to 10$\mu$m. The drag flow rate is 2 l/min and other parameters are the same as the experimental device.

and Ethanol when it is scaled lengths of the detectors to 100$\mu$m, the potential of detection to 180 V and localization of ion generation to 10$\mu$m. The other parameters match those of the experimental device.

## 7. Conclusions

In this work we first introduce the species identification-by-mobility issue via standard cross-flow method when trying to scale to submillimeter sizes. We propose a manufacturing method with micro-system technology which faces the issue in an original way. We analyze thoroughly the corona discharge and verify Peek's law in the micro-scale. With this, we have dimensioned the geometry for the proposed ionizer to localize the ion generation in order to implicitly focalize ions entry to the detection zone in a smaller size than the drift length. At the same time, we analyzed the system's flow to design ion transportation from its generation point to its detection point. By introducing orthogonal movements we have made numeric simulations to analyze viscosity effects and state experimental configuration to guarantee the laminar flux condition. We found a simplified design for the micro-system channel's construction that avoids expansions or contractions. In this way, turbulence and stopped-flow zones are minimized in an adequate flow range which allowed optimizing the device's functioning. We performed experiments on a prototype with said design that allowed us to verify our hypothesis on localized ion-generation. Variation of the average trajectory of the ion stream with the variation of drift velocity can be analyzed with a parabolic velocity profile. We show for case in which variations of drift velocity are 25% allow signal with negligible overlapping in $1mm$ on the detection zone. For lesser differences as the ones in other volatile compounds we would need to adjust the analyzed parameters in this work, which depends on the application of the device, but not on the architecture of design. We have proposed a bound for the size of the lobes of ions in terms of total drift length and its mobilities ratio that can ensure separability of analytes. Finally, we note that our design is substantively simplified compared to other complex solutions [9, 10], here we have only used tools given by micro-system design - obtaining a compact model with the advantages of no radioactive sources, performing ionic generation via a $1kV$ electrical source.

## 8. Acknowledgments

This work was supported by ANPCyT-FONCyT (grants PAE 22594/2004 and PAE-PAV 22592/2004 nodo NEA:23016 and nodo CAC:23831). We acknowledge useful comments of Jessica Lasorsa.

## References

[1] Ortiz GP, Rinaldi C, Boggio N, Vorobioff J, Ortiz J, Gómez S, et al. *Development of an IMS Type Device for Volatile Organic Compounds Detection: Simulation and Comparison of the Ion Distributions.* Physics.Ins-De [internet]. 2009 Mar 29 [2012 Jan 10];0902.1206v2. Available from http://arxiv.org/abs/0902.1206.

[2] Vinopal R, Jadamec J, de Fur P, Demars A, Jakubielski S, Green C, et. al. *Fingerprinting bacterial strains using ion mobility spectrometry.* Elsevier. Anal. Chim. Acta. 2002; 21745:1-13.

[3] Mang Zhang, Anthony S. Wexlerk. *Cross-flow ion mobility spectrometry: Theory and initial prototype testing*, Int. J. Mass Spectrom. 2006, 258(1-3):13-20.

[4] Boggio N, Alonso P, Ortiz J, Rinaldi C, Lamagna A, Boselli A. *Desarrollo de un espectrómetro por movilidad iónica para la detección de compuestos orgánicos (explosivos, drogas y contaminantes).* ANALES AFA ISSN 1850-1158. 2008;20(208):208-210.

[5] Solis A and Sacristan E. *Designing the measurement cell of a swept-field differential aspiration condenser*,Rev. Mex. Fís. 2006 Mar 22;52(4):322-328.

[6] Eiceman GA and Karpas Z. *Ion Mobility Spectrometry.* 2nd. Boca Raton:CRC Press; 2005, 350.

[7] Roscioli K, Davis E, Siems W, Mariano A, Su W, et al. *Modular Ion Mobility Spectrometer for explosives Detection Using Corona Ionization*, Anal. Chem. 2011 Aug 1; 83(15):5965-71.

[8] Sabo M and Matejek S, 2011 *Ion Mobility Spectrometry for Monitoring High-Purity Oxygen*, Anal Chem, 2011; 83 (6), 1985-1989.

[9] Zimmermann S, Abel N, Baether W, Barth S, 2007 *An ion-focusing aspiration condenser as ion mobility spectrometer*, 2007. ScienceDirect, Sensors and Actuators B, 125; 428-434.

[10] Barth S, Zimmermann S, *Modeling Ion Motion in a Miniaturized Ion Mobility Spectrometer*. In: COMSOL Conference. Proceedings of the COMSOL Conference; 2008; Hannover.

[11] Rosasa G, Murphya R, Morenob W. *Smart Antenna using MTM-MEMS.Wireless and Microwave Technology Conference (WAMICON).* In IEEE 11th Annual; 2010; Melbourne, FL. IEEE Explorer, 2010 (ISBN: 978-1-4244-6688-7) 12-13 April 2010.

[12] Ortiz J, Lamagna A, Boselli A.*Design of a CF-IMS (Cross Flow Ion Mobility Spectrometry) with MEMS technology*,Procedings of the 13th International Meeting on Chemical Sensors, 2010 July 11-14; Perth Western, ISBN: 978-1-74052-208-3, pag.332.

[13] MEMS and Nanotechnology Exchange (MNX) [internet]. Reston, Virginia. [update 1999, cited 2011] Available from: www.memsnet.org/mems/processes/deposition.html.

[14] Senturia S. *Microsystem Design.*1ed. New York: Kluwer Academic Publishers; 2000, 716.

[15] Escuela Superior de Ingenieria [internet]. Sevilla. [update 2005, cited 2011] Available from: http://iecon02.us.es/ASIGN/SEA/.

[16] M. Goldman, A. Goldman and E.S. Sigmon. *The corona discharge, its properties and specific uses* , Pure & Appl Chem. 1985; 57(9):1353-1362 .

[17] Stearns R. *The positive corona in air: A simplified analytic approach* , J of Appl Phys 1989; 66(7): 2899-2914.

[18] Azzerboni B, Cardelli E, Esposito N, Raugi M. ,Tellini A. *Three Dimensional Electromagnetic Field Due to Electric Discharge by an Analytical Approach*, IEEE Trans. Magn. 1994 Sep; 30(5):3052-55.

[19] Peek F. *Dielectric Phenomena in High Voltage Engineering.* 1er. New York:McGraw-Hill Book Company, Ink; 1920, 281 p.

[20] Krantz S. *Handbook of Complex Variables.* 1er. Boston:Birkhauser; 1999, 290.

[21] COVENTOR [internet]. North Carolina. [update 2000, cited 2010]. Available from: http://www.coventor.com/solutions/resonators/.

[22] Borg X. *Full analysis & design solutions for EHD Thrusters at saturated corona current conditions*, The General Science Journal, 2004 Jan 1. Available from: http://blazelabs.com/pdflib.asp.

[23] Ortiz J, Nigri C, Rodrigez D, Ortiz G, Perillo P, Lasorsa C, et al. *Verification of Paschen curve and Peek's Law in Micro Glow-discharge.* Proceding of the II Congreso de Microelectrónica y Aplicaciones (uEA), 2011 Sep 6-9. La Plata, Argentina. ISBN 978-950-34-0749-3, pag. 235-237.

[24] Friedrich Paschen. *Ueber die zum Funkenubergang in Luft, Wasserstoff und Kohlensaure bei verschiedenen Drucken erforderliche Potentialdifferenz* Annalen der Physik, 1889 273(5):69–75,48-56.

[25] H. F. Tammet, *The Aspiration Method For Determination Of The Determination Of Atmospheric-Ion Spectra*, Scientific Notes of Tartu State University, 1967 2(195):1-9.

[26] Raizer Y. *Gas Discharge Physics.* 1ed Springer. Springer; 1991 Sep 19, 449.

[27] The numerical calculation was done through Laplace's equation extended to the entire volume. The algorithm used is called P-FFT (precorrected fast Fourier transform) [20] impose conditions of symmetry on the top and sides of the volume. At the bottom edge conditions are voltage to the electrodes, positive on nails and zero for the plane, while the bottom surface charge surface boundary conditions on which find electrodes is zero [21].